2020

Magneto-Driven Gradients of Diamagnetic Objects for Engineering Complex Tissues

Hannah M. Zlotnick
University of Pennsylvania

Andy T. Clark
Bryn Mawr College, atclark@brynmawr.edu

Sarah E. Gullbrand
University of Pennsylvania

James L. Carey
University of Pennsylvania

Xuemei Cheng
Bryn Mawr College, xcheng@brynmawr.edu

See next page for additional authors

Citation

Zlotnick, H. M., Clark, A. T., Gullbrand, S. E., Carey, J. L., Cheng, X. M. and Mauck, R. L. 2020. "Magneto-Driven Gradients of Diamagnetic Objects for Engineering Complex Tissues." *Advanced Materials* 2005030.

Magneto-Driven Gradients of Diamagnetic Objects for Engineering Complex Tissues

*Hannah M. Zlotnick, Andy T. Clark, Sarah E. Gullbrand, James L. Carey, Xuemei Cheng, Robert L. Mauck**

H. M. Zlotnick, Prof. R. L. Mauck
Department of Bioengineering
School of Engineering and Applied Science
University of Pennsylvania
Philadelphia, PA 19104, USA
E-mail: lemauck@pennmedicine.upenn.edu

H. M. Zlotnick, S. E. Gullbrand, Prof. J. L. Carey, Prof. R. L. Mauck
McKay Orthopaedic Research Laboratory
Department of Orthopaedic Surgery
Perelman School of Medicine
University of Pennsylvania
Philadelphia, PA 19104, USA

H. M. Zlotnick, S. E. Gullbrand, Prof. R. L. Mauck
Translational Musculoskeletal Research Center
Corporal Michael J. Crescenz VA Medical Center
Philadelphia, PA 19104, USA

A. T. Clark, Prof. X. Cheng
Department of Physics
Bryn Mawr College
Bryn Mawr, PA 19010, USA

Keywords: magnetic fields, gradients, cell patterning, hydrogels, tissue engineering

Abstract

Engineering complex tissues represents an extraordinary challenge and, to date, there have been few strategies developed that can easily recapitulate native-like cell and biofactor gradients in three-dimensional materials. This is true despite the fact that mimicry of these gradients may be essential for the functionality of engineered graft tissues. Here, a non-traditional magnetics-based approach is developed to predictably position naturally diamagnetic objects in 3D hydrogels. Rather than magnetizing the objects within the hydrogel, the magnetic susceptibility of the surrounding hydrogel precursor solution is enhanced. In this way, a range of diamagnetic objects (e.g. polystyrene beads, drug delivery microcapsules, and living cells) are patterned in response to a brief exposure to a magnetic field. Upon photo-crosslinking the hydrogel

precursor, object positioning is maintained, and the magnetic contrast agent diffuses out of the hydrogel, supporting long-term construct viability. This approach is applied to engineer cartilage constructs with a depth-dependent cellularity mirroring that of native tissue. To the best of the knowledge, these are the first results showing that magnetically unaltered cells can be magneto-patterned in hydrogels and cultured to generate heterogeneous tissues. This work provides a foundation for the formation of opposing magnetic susceptibility-based gradients within a single continuous material.

Main Text

For decades, tissue engineers have focused on creating tissues to replace or model highly complex, heterogeneous tissues.[1,2] In certain cases, the simplified, homogeneous, models created by standard fabrication methods may suffice, however graft functionality and model system relevance are both enhanced by improved biomimicry. Early work on the development of gradient scaffolds showed efficacy, but widespread applicability was limited by the need for specialized materials and fabrication techniques.[3,4] The advent and subsequent refinement of three-dimensional (3D) bioprinting significantly improved capabilities for engineering tissues with spatial heterogeneities. However, print resolution (~100 μm) currently limits the detail and continuity of deposited features.[5] Other techniques, such as photopatterning, offer greater spatial control of material cues, which can then influence cell phenotype, but again, photopatterning relies on specialized photoresponsive materials.[6,7]

More recently, researchers have developed other precise patterning techniques—buoyancy, acoustic, and magnetic patterning—that work across a wide range of materials (e.g. hydrogels) and objects (e.g. cells, growth factors, microspheres, etc.).[8–12] These methods rely on a differential between the object and material property of interest, *x*, where *x* refers to the density (buoyancy patterning), density and compressibility (acoustic patterning), or magnetic susceptibility (magnetic patterning). Unlike unidirectional buoyancy-driven gradients and

geometric acoustic patterns, magnetic fields have the potential to create multidirectional 3D patterns. **Equation 1** must be valid to enable patterning:

$$x_{\text{object}} - x_{\text{material}} \neq 0 \quad (1)$$

A greater difference in x improves the ease and speed of patterning, if this force (i.e. the magnetic force) is dominant over opposing forces—most commonly including gravitational and drag forces. However, most objects and materials are similarly diamagnetic and do not create a significant differential in x to overcome opposing forces. Therefore, magnetic patterning (magneto-patterning) approaches traditionally require the object to be magnetically tagged.[10,11] Unfortunately, not all objects are receptive to magnetic tags; for example, intracellular iron oxide particles can compromise cell differentiation.[10,12] Ideally, an object could be magnetically manipulated without altering its intrinsic magnetic character.

In this work, we developed a magnetics-based approach to position unaltered cells, or any diamagnetic objects of interest, within 3D hydrogels. Previously, magnetics-based approaches have been developed and employed to separate different cell populations in 2D,[14] levitate cells,[15] and assemble cell aggregates without magnetically tagging the cells.[16] To carry out these studies, the magnetic susceptibility of the cell-containing solution was enhanced, increasing x_{material}. However, to the best of our knowledge, this concept of altering x_{material} (instead of x_{object}) has not been applied to magneto-pattern diamagnetic objects in 3D, and subsequently fix this pattern by crosslinking the surrounding solution. Here, we show that the addition of a gadolinium-based magnetic contrast agent to a hydrogel precursor solution effectively (and transiently) increases x_{material}, satisfying Equation 1, and allowing a variety of diamagnetic objects to be magnetically manipulated. After positioning the objects, we crosslinked the hydrogels, and serially washed the samples to elute the magnetic contrast agent. By incorporating quantitative parameters associated with our experimental setup, we were able to show that the magnetophoretic mobility of objects is computationally predictable in this system. This computational simulation established a working parameter space for our

experimental trials. We then demonstrated the versatility of our approach by patterning diamagnetic objects of different sizes, including polystyrene beads, poly($_{D,L}$-lactide-*co*-glycolide) (PLGA) microcapsules, and mesenchymal stromal cells (MSCs). We next applied our magneto-patterning method to the field of complex tissue engineering by generating engineered cartilage constructs with a depth-dependent cellularity similar to native articular cartilage. We mimicked the continuous high-to-low cellularity observed in articular cartilage from the superficial (top) region to the deep (bottom) region of the tissue. The initial viability and metabolic activity of these constructs over 6 weeks of *in vitro* culture was not impacted by the brief magnetic field exposure during construct fabrication. More importantly, the biochemical gradient of these constructs corresponded with the local cellularity, as assessed histologically at 3 weeks, and quantitatively at 6 weeks. The predictability and versatility of our magneto-patterning approach should enable future applications to the field of complex tissue engineering, particularly toward the fabrication of tissues with opposing cell and biofactor gradients.

Since previous studies magnetically manipulating diamagnetic objects were limited to 2D and/or nonviscous solutions,[14–17] we first sought to establish whether 3D manipulation in viscous solutions was theoretically possible, and if so, under what parameter space. To do this, we first established our experimental magneto-patterning workflow (**Figure 1**A). In this workflow, one or more diamagnetic objects are combined with a hydrogel precursor solution (1% w/v methacrylated hyaluronic acid, MeHA), a magnetic contrast agent (200 x 10^{-3} M Gadodiamide, Gd), and a photoinitator (0.5% w/v Lithium phenyl-2,4,6-trimethylbenzoylphosphinate, LAP). This crosslinkable viscous solution is then injected into a mold (∅: 4 mm, height: 1.3 mm) 3.8 mm above a permanent magnet (∅: 15/16”, height: ½”, B_{rmax}: 13,200 Gauss). After a set time of magnetic field exposure, the solution is photocrosslinked, locking the objects in place. To model this system computationally, we started by mapping the magnetic field across a 2D cross section of the gel, using the COMSOL

Multiphysics software (Figure 1B). Throughout this cross section, the magnetic field is relatively constant in the R-direction, and decreases in the Z-direction from 340 mT (Z: 0 mm) to 280 mT (Z: 1.3 mm). The uniformity of the magnetic field in the R-direction is due to the fact that the diameter of the magnet is ~6-fold larger than the diameter of the gel. We exported the magnetic field map from the COMSOL software into MATLAB to calculate the magnetic force (F_{mag}) on an object at a given point in the viscous solution. Along with F_{mag}, we also accounted for the buoyant (F_{buoy}), gravitational (F_{grav}), and drag (F_{drag}) forces in our simulation (Figure 1C). For a known object, these force equations (Supporting Information) were iteratively solved until the object reached the top of the solution, or until the simulation reached the set maximum magnetic field exposure time (10 minutes). The experimental parameters used in the simulation are outlined in Table S1 of the Supporting Information.

In addition to implementing our experimental parameters in our computational model, we also explored a range of solution viscosities (Figure S1, Supporting Information), and magnetic susceptibilities (Figure S2, Supporting Information) to characterize the constraints of the magneto-patterning approach. We performed these analyses for two cases. The first case is when the solution is slightly denser than the object, and there is a minor buoyant contribution to the upward motion of the objects:

$$\rho_{\text{object}} - \rho_{\text{solution}} = -0.01 \text{ g mL}^{-1} \quad (2)$$

The second case is when the object is slightly denser than the solution, and there is a minor gravitational contribution to the net force on the objects:

$$\rho_{\text{object}} - \rho_{\text{solution}} = +0.01 \text{ g mL}^{-1} \quad (3)$$

From this analysis, we found that for both **Equation 2** and **Equation 3**, solutions that are ten-fold more viscous than water at 20°C are able to facilitate object patterning in under 10 minutes. Additionally, the system is sensitive to the concentration of Gadodiamide in the solution. Objects in a solution with only 1 x 10^{-3} M Gadodiamide exhibited little movement, especially in

the case where the object is more dense than the solution (Equation 3). To increase the speed of patterning, the concentration of Gadodiamide, or the magnetic field strength can be increased.

Through this simulation, we discovered that the radius of the diamagnetic object has a large influence on its magnetophoretic mobility within the paramagnetic fluid (Figure 1D). Small objects (radius: 1 μm) experience little to no movement in our system, mainly because F_{mag} is so small. Larger objects (radius: 5-15 μm) of the same density ascend to the top of the solution after 10 minutes of magnetic field exposure (Figure 1D, E). This upward movement is primarily due to F_{mag}, and not F_{buoy}. Indeed, an object can be magneto-patterned even if it is denser than the surrounding solution (Figure S1, Supporting Information).

While our magneto-patterning approach eliminates the need for magnetically tagging objects, such objects could be patterned opposite diamagnetic objects in this system. We extended our computational model to illustrate this concept of magnetic susceptibility based multi-directional patterning (Figure 1F). The motion direction of the objects is determined by the resultant net force from the vector sum of the forces outlined in Figure 1C. As diamagnetic objects ($\chi < 0$) move toward regions of low magnetic field strength, paramagnetic objects (χ: 10^{-4}-10^{-2}) move toward regions of high magnetic field strength. Therefore, within the same weakly paramagnetic solution (χ: 10^{-5}), diamagnetic objects would cross paths with paramagnetic objects, ultimately creating opposing gradients.

Our computational model supported the feasibility of magneto-patterning diamagnetic objects in 3D viscous solutions, and we progressed to experimentally validate this computational finding by positioning a range of objects in our system. We separately tested the movement of three different diamagnetic objects: polystyrene beads (radius: 5 μm, ρ: 1.05 g mL^{-1}), drug delivery microcapsules (radius: 20 μm), and living MSCs (**Figure 2**A). To do this, we followed our established workflow (Figure 1A), to create a crosslinkable viscous solution

(1% w/v MeHA, 0.05% w/v LAP) containing our object of interest, and the magneto-responsive fluid (200 x 10^{-3} M Gd). The solution was injected into a mold, exposed to the magnetic field (Figure 1B) for up to 10 minutes, and subsequently crosslinked with UV light (λ: 365 nm, intensity: 10 mW cm^{-2}, 9 minutes). We diametrically sectioned the gels to visualize the distribution of magneto-patterned objects within a 2D cross section, similar to the visualization from our computational model. The distribution of polystyrene beads in the magneto-patterned gels (Figure 2B) resembled our model output (Figure 1E), where after 10 minutes of magnetic field exposure, the majority of the beads had reached the top of the gel. Interestingly, the drug delivery microcapsules, composed of an outer PLGA shell and inner aqueous depot, moved faster, but more unevenly, than the polystyrene beads (Figure 2C). We attribute this variability in the movement of the microcapsules to intra-batch differences.[18,19] While all of the microcapsules are fabricated from the same microfluidic device, there are inherently minor differences in shell thickness and microcapsule diameter within the batch. Additionally, small defects in the shells of the microcapsules would allow the magnetic susceptibility modifier to flow from the viscous solution into the capsules, thereby negating Equation 1. Nevertheless, the majority of microcapsules responded to the applied magnetic field, showing that a therapeutic cargo could be positioned in a gradient fashion using this approach.

Next, we aimed to magneto-pattern living, unaltered MSCs in 3D hydrogels. More specifically, we sought to create a cellular gradient within the gels, so as to match the depth dependence in cellularity in native tissue. Here, we used MSCs (bovine, passage 2, 20 million cells mL^{-1}) as the objects of interest within our Gd-containing crosslinkable viscous solution. We also added small polystyrene beads (radius: 0.5 μm) to this solution as fiducial markers. As we learned from our computational model, objects with a radius below 1 μm are non-responsive to the applied magnetic field (Figure 1D), and so, these small beads marked the boundaries of the gels. After magneto-patterning the MSCs, we serially washed the cell-laden gels to promote Gd release and cell viability; this wash procedure was confirmed to effectively elute the Gd

(Supporting Information, Figure S3). We then cultured the magneto-patterned gels for 2 days *in vitro*, and subsequently imaged the constructs to assess the distribution and viability of the MSCs. In the control gels that were not exposed to the magnetic field, cellularity was constant throughout the depth of the samples (Figure 2D, E). However, in the gels that were exposed to the magnetic field for 10 minutes, there was a clear cellular gradient from the top to the bottom of the samples, which was validated by regional quantification of cell density. This regional quantification also demonstrated the repeatability of our approach, as the standard deviations for each group (0, 2, 5, 10 min) in a given region are small. Additionally, at this timepoint, cell viability was unaltered by the magnetic field exposure (Supporting Information, Figure S4).

Having successfully demonstrated that we could magneto-pattern living MSCs, and that the construct fabrication process maintained cell health, we next sought to apply our method to engineer articular cartilage, which has a natural cellular gradient from the superficial (high cellularity) to the deep zone (low cellularity) of the tissue.[20] While there have been numerous gradient tissue engineering studies that focus on regenerating the sharp interface between cartilage and bone,[3,8] few have engineered the depth-dependent composition of articular cartilage itself, without discrete material interfaces. Since our magneto-patterning approach 1) eliminates the need for permanent, potentially toxic magnetic tags, and 2) relies instead on Gd that washes out of the constructs within 24 h (Supporting Information, Figure S3), it is particularly conducive to fabricating tissue constructs for long-term culture. We generated control constructs (no magnetic field exposure), and constructs that received either 2 or 5 minutes of magnetic field exposure for a 6-week culture in chondrogenic media (**Figure 3**A). The 10-minute condition, as shown in Figure 2D, was not selected due to the paucity of cells in the bottom region of the gels. We tracked the metabolic activity of the constructs over time in culture (Day 1, 14, 28, 42 timepoints) using an Alamar Blue assay. There were no differences between construct groups within a timepoint. All of the groups trended upward with time, signifying increased metabolic activity, and overall construct vitality (Figure 3B). After 3 weeks

of culture, constructs stained with Alcian Blue indicated that proteoglycan deposition (Figure 3C) corresponded with the local, patterned cellularity of the constructs (Figure S5, Supporting Information). The 5 min constructs had noticeably less proteoglycan staining in the bottom region. At the terminal timepoint (6 weeks), we divided the constructs into top and bottom regions, measured their wet weights, and enzymatically digested each region. For a given pair (top and bottom) (Figure S6, Supporting Information), we computed the ratio of a major cartilage extracellular matrix component, glycosaminoglycan (GAG, normalized by wet weight), of the bottom region to the GAG content of the top region (Figure 3D). We did not detect a difference between the 2 min and control groups for this measure, likely due to the sensitivity of the assay and subtle gradients formed under these conditions. The cellular gradient created in the 2 min constructs is mainly localized to the bottom 20% of the constructs (Figure 2D, E). Conversely, and consistent with our histological assessment at 3 weeks, this GAG ratio was statistically different for the 5 min patterning condition, compared to the control. This finding is particularly exciting, and shows the promise of our magneto-patterning approach in generating cellular gradients that culminate in matrix gradients. Taken together, the metabolic tracking, histology, and regional GAG quantification show that magneto-patterned MSCs can thrive, produce cartilaginous matrix, and establish matrix gradients over long term culture. Moving forward, we will seek to apply the opposing magneto-induced gradients (depicted in Figure 1F) to generate tissue constructs with opposing populations of chondrogenic cells and magnetically tagged bone-promoting agents. Reducing this to practice holds the potential to create continuous osteochondral tissues that lack sharp material discontinuities through the depth.

In conclusion, we established an innovative magneto-patterning approach that allows diamagnetic objects, including living cells, to be predictably positioned in 3D hydrogels in response to the brief application of a magnetic field *without* magnetically tagging the objects. We instead altered the magnetic susceptibility of the viscous hydrogel precursor solution,

causing a range of diamagnetic objects (polystyrene beads, drug delivery microcapsules, and MSCs) to be repulsed from a permanent magnet. Most importantly, after crosslinking the gels to 'lock in' the object positions, we showed that the magnetic contrast agent diffused out of the hydrogels, supporting the long-term health and viability of the cell-laden constructs. We extended this approach to fabricate engineered cartilage constructs with a high cellularity in the top region, and a low cellularity in the bottom region, similar to native tissue. Over long-term culture, the constructs maintained these cellular gradients, and subsequently produced gradients in the extracellular matrix content. Overall, the predictability and versatility of this magneto-patterning approach will enable engineers to design and create complex tissues by simply combining their hydrogel and objects of choice.

Supporting Information
Supporting Information is available from the Wiley Online Library or from the author.

Acknowledgements
This project was supported by the National Institute of Health (R01 AR056624, R01 AR071340, T32 AR007132, P30 AR069619) and the Department of Veterans Affairs (IK6 RX003416). Additional support was provided by the NSF Center for Engineering Mechanobiology (CMMI: 15-48571). The authors would also like to acknowledge Dr. Stephen Pickup and the University of Pennsylvania Small Animal Imaging Facility where all MRI testing was performed, and Ana Peredo, Dr. Daeyoon Lee, and Dr. George Dodge for input on microcapsules.

Conflict of Interest
H.M.Z, A.T.C, X.C., and R.L.M. are inventors on a patent application (US Provisional Application No. 63/009,419) related to the technology described in this paper.

Author Contributions
H.M.Z., A.T.C, X.C., and R.L.M. conceived the idea and designed the experiments. H.M.Z. performed the majority of experimental work. A.T.C. assisted with magnetic field modeling, and S.E.G. assisted with magnetic resonance imaging. J.L.C, X.C., and R.L.M supervised the project.

Received: ((will be filled in by the editorial staff))
Revised: ((will be filled in by the editorial staff))
Published online: ((will be filled in by the editorial staff))

References

[1] R. L. Mauck, M. A. Soltz, C. C. B. Wang, D. D. Wong, P. H. G. Chao, W. B. Valhmu, C. T. Hung, G. A. Ateshian, *J. Biomech. Eng.* **2000**, *122*, 252.

[2] J. Kisiday, M. Jin, B. Kurz, H. Hung, C. Semino, S. Zhang, A. J. Grodzinsky, *Proc. Natl. Acad. Sci.* **2002**, *99*, 9996.

[3] N. Mohan, N. H. Dormer, K. L. Caldwell, V. H. Key, C. J. Berkland, M. S. Detamore, *Tissue Eng. Part A* **2011**, *17*, 2845.

[4] S. H. Oh, T. H. Kim, J. H. Lee, *Biomaterials* **2011**, *32*, 8254.

[5] M. E. Prendergast, J. A. Burdick, *Adv. Mater.* **2020**, *32*, 1.

[6] S. Khetan, J. A. Burdick, *Biomaterials* **2010**, *31*, 8228.

[7] K. A. Mosiewicz, L. Kolb, A. J. Van Der Vlies, M. M. Martino, P. S. Lienemann, J. A. Hubbell, M. Ehrbar, M. P. Lutolf, *Nat. Mater.* **2013**, *12*, 1072.

[8] C. Li, L. Ouyang, I. J. Pence, A. C. Moore, Y. Lin, C. W. Winter, J. P. K. Armstrong, M. M. Stevens, *Adv. Mater.* **2019**, *1900291*, 1.

[9] J. P. K. Armstrong, J. L. Puetzer, A. Serio, A. G. Guex, M. Kapnisi, A. Breant, Y. Zong, V. Assal, S. C. Skaalure, O. King, T. Murty, C. Meinert, A. C. Franklin, P. G. Bassindale, M. K. Nichols, C. M. Terracciano, D. W. Hutmacher, B. W. Drinkwater, T. J. Klein, A. W. Perriman, M. M. Stevens, *Adv. Mater.* **2018**, *30*, 1.

[10] S. P. Grogan, C. Pauli, P. Chen, J. Du, C. B. Chung, S. D. Kong, C. W. Colwell, M. K. Lotz, S. Jin, D. D. D'Lima, *Tissue Eng. Part C Methods* **2012**, *18*, 496.

[11] C. Li, J. P. Armstrong, I. J. Pence, W. Kit-Anan, J. L. Puetzer, S. Correia Carreira, A. C. Moore, M. M. Stevens, *Biomaterials* **2018**, *176*, 24.

[12] C. Li, L. Ouyang, M. M. Stevens, J. P. K. Armstrong, *Trends Biotechnol.* **2020**, 1.

[13] L. Kostura, D. L. Kraitchman, A. M. Mackay, M. F. Pittenger, J. M. W. Bulte, *NMR Biomed.* **2004**, *17*, 513.

[14] F. Shen, H. Hwang, Y. K. Hahn, J. K. Park, *Anal. Chem.* **2012**, *84*, 3075.

[15] N. G. Durmus, H. C. Tekin, S. Guven, K. Sridhar, A. Arslan Yildiz, G. Calibasi, I. Ghiran, R. W. Davis, L. M. Steinmetz, U. Demirci, *Proc. Natl. Acad. Sci.* **2015**, *112*, E3661.

[16] A. Tocchio, N. G. Durmus, K. Sridhar, V. Mani, B. Coskun, R. El Assal, U. Demirci, *Adv. Mater.* **2018**, *30*, 1.

[17] K. A. Mirica, F. Ilievski, A. K. Ellerbee, S. S. Shevkoplyas, G. M. Whitesides, *Adv. Mater.* **2011**, *23*, 4134.

[18] B. Mohanraj, G. Duan, A. Peredo, M. Kim, F. Tu, D. Lee, G. R. Dodge, R. L. Mauck, *Adv. Funct. Mater.* **2019**, *29*, 1.

[19] A. P. Peredo, Y. K. Jo, G. Duan, G. R. Dodge, D. A. Lee, R. L. Mauck, *Biomaterials* **2020**, *in press*.

[20] K. D. Jadin, B. L. Wong, W. C. Bae, K. W. Li, A. K. Williamson, B. L. Schumacher, J. H. Price, R. L. Sah, *J. Histochem. Cytochem.* **2005**, *53*, 1109.

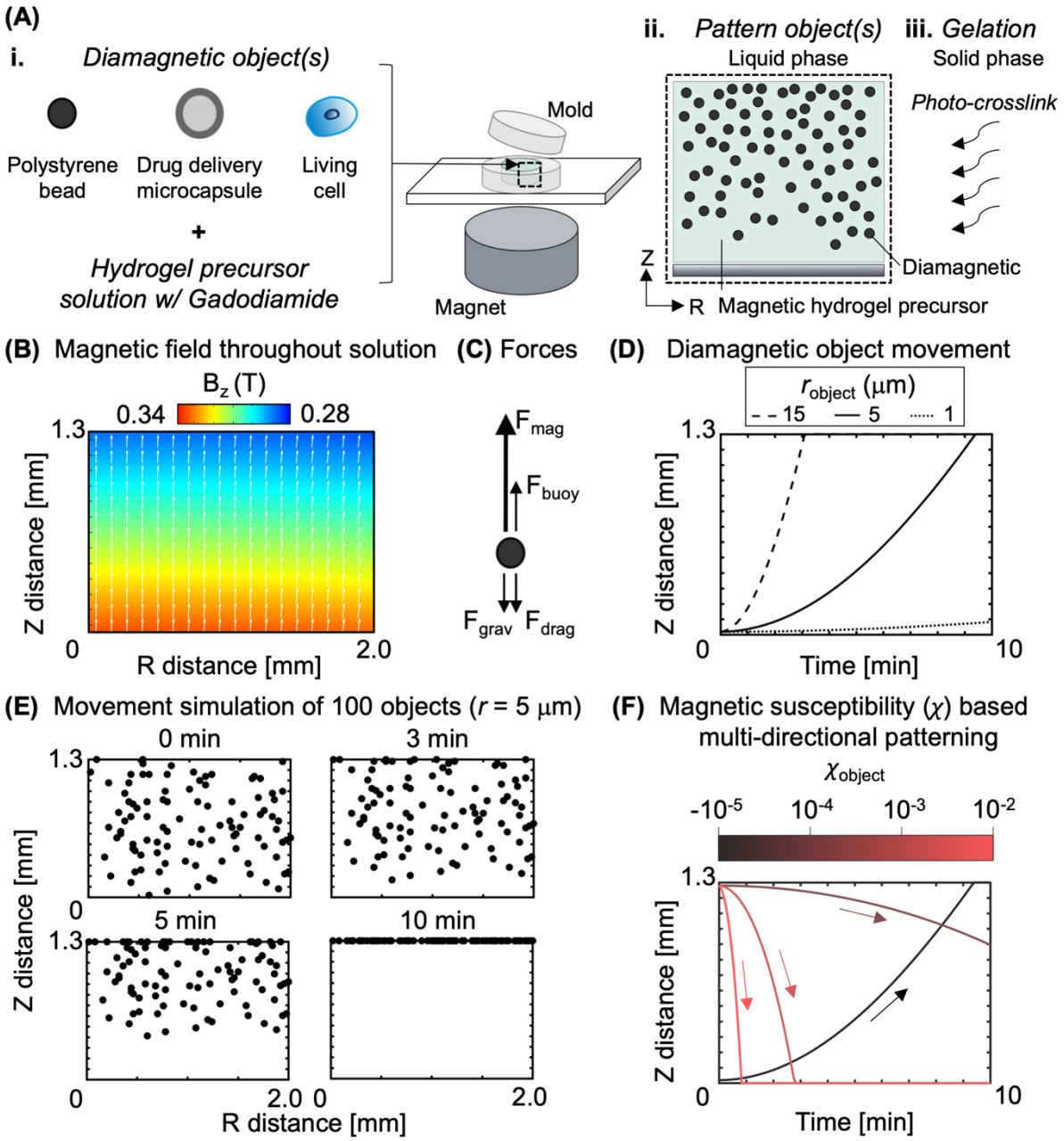

Figure 1. Enhancing the magnetic susceptibility of a hydrogel precursor enables positioning of diamagnetic and paramagnetic objects. (A) Schematic of magneto-patterning setup. i) The object(s) of interest are combined with a hydrogel precursor, gadodiamide, and a crosslinker. ii) The objects(s) are patterned under brief application of a magnetic field. iii) Gelation is induced to immobilize the object(s). (B) COMSOL model of the magnetic field across a diametric cross-section of the hydrogel using a single permanent magnet (15/16" diameter, B_{rmax} = 1.32 T). (C) Free body diagram of forces on a diamagnetic object within a paramagnetic solution. (D) MATLAB simulation of polystyrene beads (1.05 g/mL density) of different radii moving in the hydrogel precursor solution. (E) Simulation of 100 objects moving over 10 minutes of magnetic field exposure. (F) Simulation of diamagnetic and paramagnetic objects (5 μm) moving within the weakly paramagnetic hydrogel precursor. Arrows indicate paths of objects.

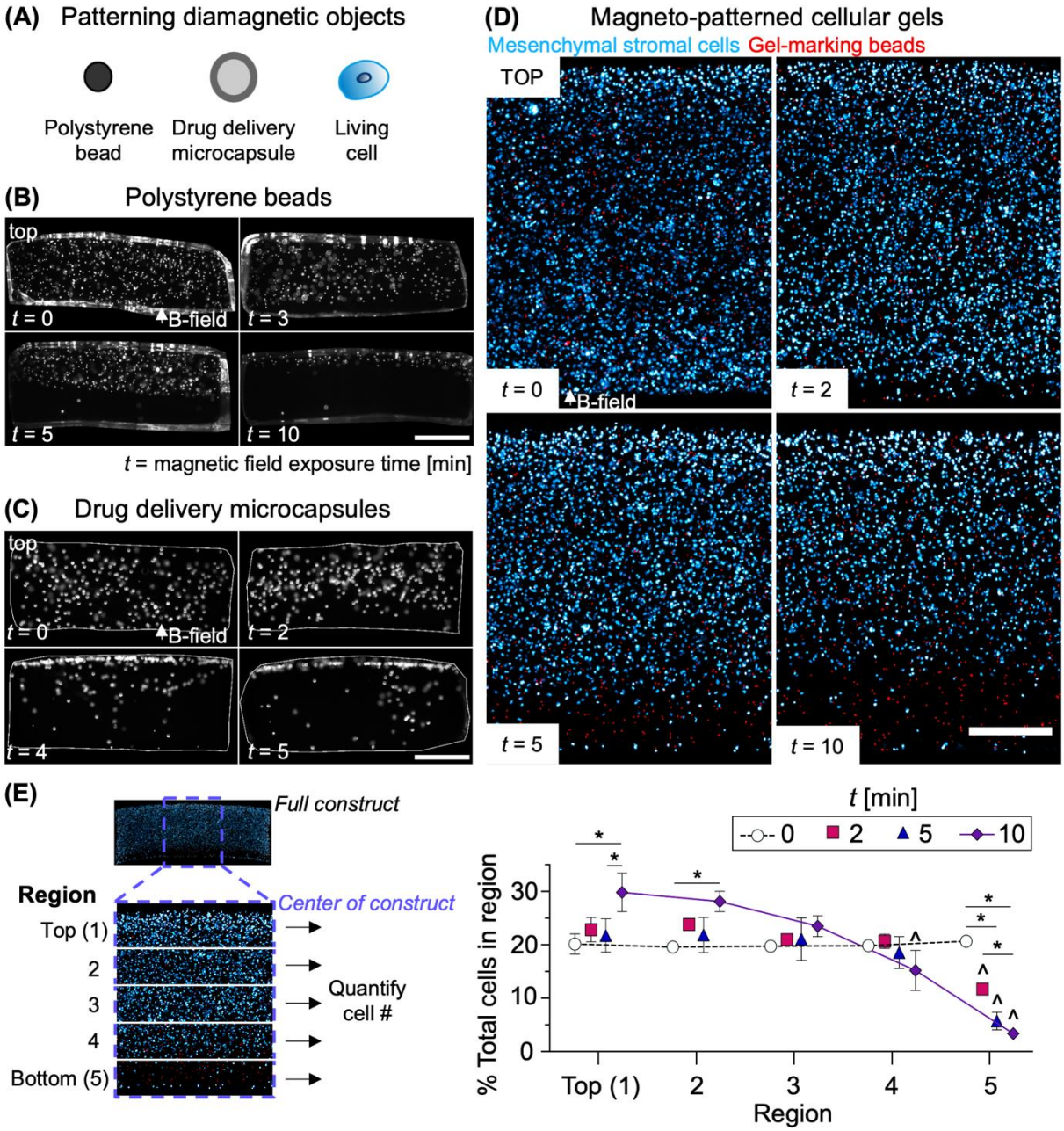

Figure 2. Engineering gradients of diamagnetic objects in hydrogels using magnetic fields. (A) Polystyrene beads (10 μm diameter, 1.05 g mL^{-1} density), poly(lactic-co-glycolic acid) microcapsules containing bovine serum albumin (40 μm diameter), and mesenchymal stromal cells (MSCs, ~20 μm diameter), are all diamagnetic and positioned using a magnetic field. (B, C) Cross-sectional view of magneto-patterned methacrylated hyaluronic acid (MeHA) hydrogels with polystyrene beads and microcapsules, respectively. Scale bars, 1 mm. *t* represents the time of exposure to the magnetic field [min] before crosslinking. (D) Cross-sectional view of magneto-patterned MSC-laden constructs stained with 4′,6-diamidino-2-phenylindole (DAPI, blue, nuclear) after 2 days of culture. Small polystyrene beads (red, 1 μm diameter, not responsive to the magnetic field) mark the gel boundary. Scale bar, 500 μm. (E) Quantification of cellularity throughout the depth of the constructs. Region 1: top of construct, furthest from magnet. Region 5: bottom of construct, closest to magnet. Data represent the mean ± standard deviation from 3 constructs (2-way analysis of variance, ANOVA, Bonferroni's multiple comparisons test), $p < 0.05$ (*, ^), * vs. exposure time within Region, ^ vs. Region 1 and Region 2 within exposure time.

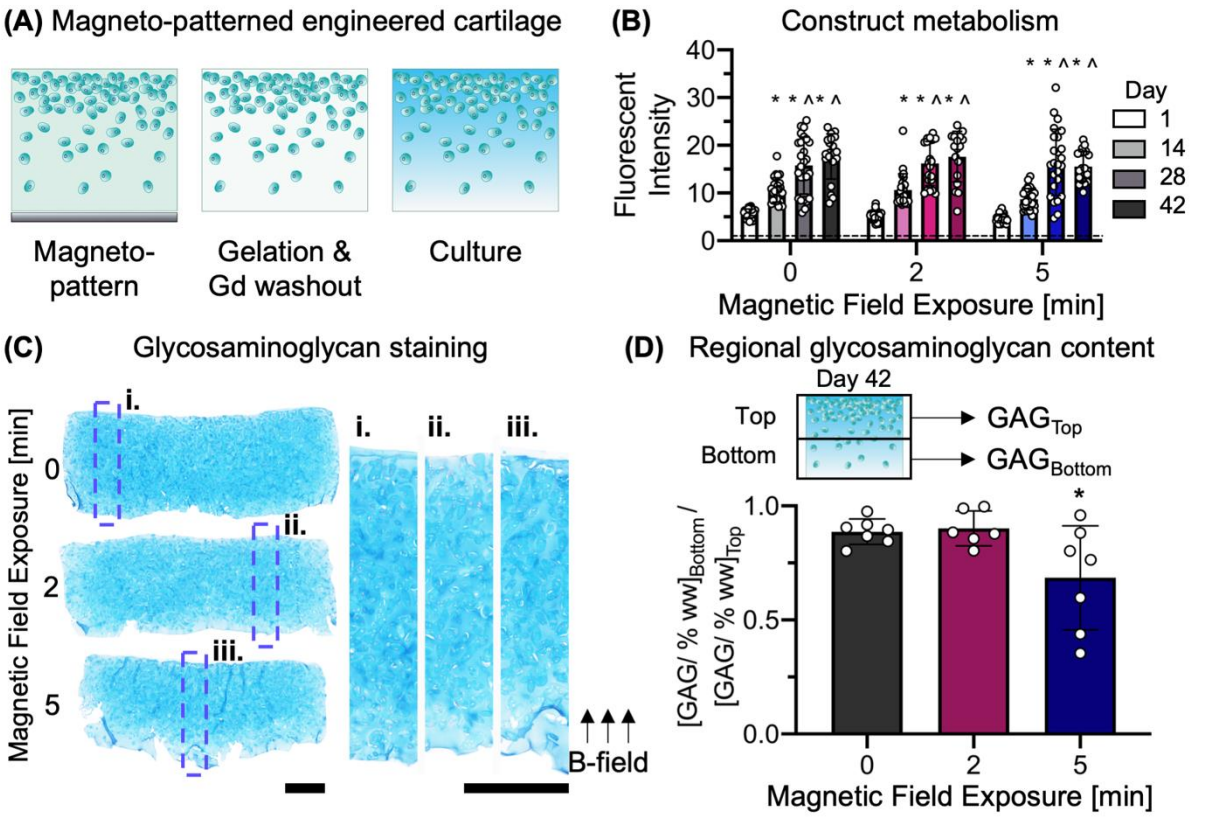

Figure 3. Engineering articular cartilage with depth dependent matrix content via cell magneto-patterning. (A) Schematic showing fabrication and culture of magneto-patterned engineered cartilage constructs. (B) Metabolism of magneto-patterned MSC-laden constructs, as assessed via an Alamar Blue Assay. The dashed line represents the fluorescent intensity of a well without a construct (media only). Data represent mean ± standard deviation from 18-26 samples/group (2-way ANOVA, Bonferroni's multiple comparisons test), $p < 0.05$ (*, ^), * vs. Day 1 within field exposure, ^ vs. Day 14 within field exposure. (C) Magneto-patterned constructs cultured for 3 weeks and stained with Alcian blue (proteoglycans). Scale bars, 500 μm. (D) Magneto-patterned constructs cultured for 6 weeks and digested in proteinase K for biochemical analysis of the top and bottom halves. Data represent the mean ± standard deviation from 6-7 samples/group (1-way ANOVA with comparisons to control—0 min, Bonferroni's multiple comparisons test), $p < 0.05$ (*), * vs. 0 min.